Microelectronics Reliability 73 (2017) 42–53

Contents lists available at ScienceDirect

Microelectronics Reliability

journal homepage: www.elsevier.com/locate/microrel

Advancement in simulating moisture diffusion in electronic packages under dynamic thermal loading conditions

Jing Wang *, Ruiyang Liu, Dapeng Liu, Seungbae Park

Department of Mechanical Engineering, State University of New York at Binghamton, Binghamton, NY 13902, United States

ARTICLE INFO

Article history:
Received 23 November 2016
Received in revised form 3 March 2017
Accepted 12 April 2017
Available online 19 April 2017

Keywords:
Moisture diffusion
Normalized concentration
Dynamic temperature
Electronic packaging

ABSTRACT

The normalization approach has been accepted as a routine to overcome the concentration discontinuity at multi-material interfaces in the moisture diffusion simulation by the finite element method. However, applying the normalization approach directly in the commercial finite element software under a dynamic thermal loading condition, such as reflow process, may lead to erroneous results. Special techniques are needed to obtain correct results. In this study, different approaches that can deal with the moisture diffusion under dynamic thermal loading conditions were reviewed and compared with case studies. Advantages and disadvantages of each approach were analyzed and discussed. Theoretical derivation was developed to show the direct concentration approach (DCA) violates the law of mass conservation. The effect of Fourier number on the accuracy of the DCA was also examined. The internal source approach was shown to be a universal method in modeling the moisture diffusion in a multi-material system under dynamic thermal loading conditions. The newest version of ANSYS also showed good performance in solving the diffusion problem under transient thermal loadings if a proper time step size was used.

1. Introduction

Plastic encapsulated IC packages are prone to absorbing moisture during the process of packaging, storage and transportation. The presence of moisture in the polymer-based materials poses significant threats to the integrity and reliability of microelectronic assemblies. Moisture can be attributed as one of the principal causes of many package failures, in particular degradation of adhesion strength and popcorn failure [1–6], etc. Therefore, understanding the behavior of moisture is essential for ensuring the durability and reliability of electronic packages.

Commercial finite element software has been commonly used by researchers to simulate the moisture-related issues in electronic packaging, such as hygroscopic swelling [7–12], vapor pressure [13–17] and interfacial delamination [18–24]. Extensive numerical studies have been conducted to investigate the moisture impact on the package reliability during the solder reflow process, but not all of the attempts can accurately predict the moisture diffusion behavior. The diffusion simulation in a multi-material system under dynamic thermal loading conditions still remains a challenge due to the complexity of enforcing the concentration continuity at the material interfaces. Several researchers proposed numerical methods to tackle this problem. In this paper, different approaches that can possibly deal with the diffusion under transient thermal loading conditions were reviewed and compared using benchmarks.

2. Background

2.1. Moisture diffusion theory

The moisture diffusion phenomenon inside polymers can be described by Fick's second law

$$\frac{\partial C}{\partial t} = \frac{\partial}{\partial x}\left(D_x \frac{\partial C}{\partial x}\right) + \frac{\partial}{\partial y}\left(D_y \frac{\partial C}{\partial y}\right) + \frac{\partial}{\partial z}\left(D_z \frac{\partial C}{\partial z}\right) \tag{1}$$

For isotropic materials ($D_x = D_y = D_z$), Eq. (1) can be simplified to

$$\frac{\partial C}{\partial t} = D\left(\frac{\partial^2 C}{\partial x^2} + \frac{\partial^2 C}{\partial y^2} + \frac{\partial^2 C}{\partial z^2}\right) \tag{2}$$

where C is the local moisture concentration, D is the diffusivity, x, y, z are coordinates and t is time.

* Corresponding author.
E-mail addresses: jwang115@binghamton.edu (J. Wang), sbpark@binghamton.edu (S. Park).

http://dx.doi.org/10.1016/j.microrel.2017.04.018
0026-2714/

The diffusivity D is a temperature-dependent material property, which can be described by the Arrhenius equation

$$D = D_0 \exp\left(-\frac{E_D}{RT}\right) \tag{3}$$

where E_D is the activation energy of the diffusivity, and D_0 is the pre-exponential factor.

The governing equation of diffusion can be solved analytically for a simple geometric model, such as a block or a sphere. However, it is quite difficult to solve the equation analytically for the model with multiple materials and complicated geometric structures, e.g., electronic packages. Usually, numerical methods using the commercial finite element software are adopted to simulate the moisture diffusion behavior inside the electronic packages. Because the governing equation for moisture diffusion is analogous to that of heat transfer, thermal-moisture analogies were used in previous studies when most finite element software did not support mass diffusion simulations. Latest versions of commercial finite element software, such as ANSYS, ABAQUS, and COMSOL, offer the mass diffusion module. Thus, there is no longer the need to use the thermal-moisture analogies to model the moisture diffusion.

2.2. Bi-material diffusion

When solving the moisture diffusion using the finite element method, one issue must be handled; that is, the moisture concentration is discontinuous at the interface of two different materials because various polymeric materials can have different moisture absorption capacities (shown in Fig. 1). In order to make the diffusion modeling numerically implementable, the normalized concentration ϕ was introduced to remove the moisture concentration continuity at material interfaces [25,26].

$$\phi = \frac{C}{S} \tag{4}$$

where S is the solubility of the material. The normalized concentration ϕ is continuous at the bi-material interface. Thus, the commercial finite element software can be utilized to perform the diffusion analysis in a multi-material system by changing the field variable from the concentration C to the normalized concentration ϕ.

A commonly-used alternative normalized concentration called "wetness" or "fractional saturation" w was introduced by Wong [27]

$$w = \frac{C}{C_{sat}} \tag{5}$$

where C_{sat} is the saturated moisture concentration. C_{sat} defines the maximum possible moisture gain per unit volume of a material at a given temperature and humidity. It is noted that C_{sat} is a function of both temperature and humidity. Based on the equality principle of chemical potential, the normalized concentration "wetness" can also be proved to be continuous at the bi-material interface (shown in Fig. 2). The above two normalization approaches are quite similar because C_{sat} can be expressed as follows:

$$C_{sat} = S \cdot P_{ext} \tag{6}$$

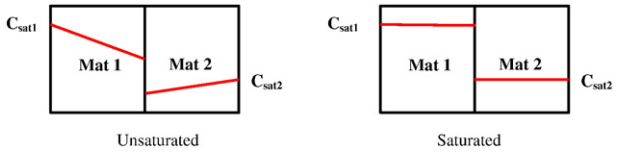

Fig. 1. Moisture concentration discontinuity at bi-material interface.

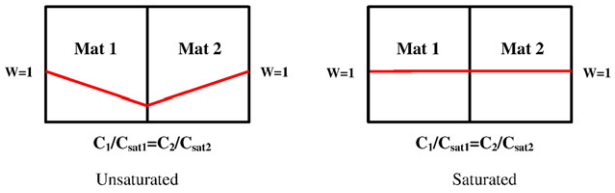

Fig. 2. Continuity of normalized concentration at bi-material interface.

where P_{ext} is the ambient vapor pressure at a given temperature and humidity.

Under a constant temperature condition such as moisture preconditioning, S or C_{sat} does not change with time, thus, the governing Eq. (2) can be written in terms of ϕ as

$$\frac{\partial \phi}{\partial t} = D\left(\frac{\partial^2 \phi}{\partial x^2} + \frac{\partial^2 \phi}{\partial y^2} + \frac{\partial^2 \phi}{\partial z^2}\right) \tag{7}$$

Similarly, the governing equation can be written in terms of w as

$$\frac{\partial w}{\partial t} = D\left(\frac{\partial^2 w}{\partial x^2} + \frac{\partial^2 w}{\partial y^2} + \frac{\partial^2 w}{\partial z^2}\right) \tag{8}$$

Under a varying temperature condition, such as reflow process, the solubility S would vary with time, and the governing equation should be expressed in the following form [28]:

$$\frac{\partial \phi}{\partial t} + \frac{\phi}{S}\frac{\partial S}{\partial t} = D\left(\frac{\partial^2 \phi}{\partial x^2} + \frac{\partial^2 \phi}{\partial y^2} + \frac{\partial^2 \phi}{\partial z^2}\right) \tag{9}$$

where

$$\frac{\partial S}{\partial t} \neq 0 \tag{10}$$

Similarly, if C_{sat} varies with time, the governing equation in terms of w becomes

$$\frac{\partial w}{\partial t} + \frac{w}{C_{sat}}\frac{\partial C_{sat}}{\partial t} = D\left(\frac{\partial^2 w}{\partial x^2} + \frac{\partial^2 w}{\partial y^2} + \frac{\partial^2 w}{\partial z^2}\right) \tag{11}$$

where

$$\frac{\partial C_{sat}}{\partial t} \neq 0 \tag{12}$$

Eqs. (9) and (11) are not easy to handle in the finite element software. For simplifying the simulation process when dealing with a varying temperature condition, C_{sat} is usually treated as a temperature-independent material property in actual simulations, so that $\partial C_{sat}/\partial t$ equals zero and Eq. (8) can be used as the governing equation. This treatment is referred to as "standard method" in this paper. The simplification is based on the discovery that there is no strong correlation between C_{sat} and the temperature for many polymer materials [29,30]. However, this holds true only within a relatively small range of temperature. It has been revealed that C_{sat} is dependent on temperature across its glass transition temperature (T_g) [31,32]. During the lead-free solder reflow, the package temperature can reach 230 °C–260 °C, which is much higher than the glass transition temperature of most polymer-based packaging materials. Under such conditions, C_{sat} cannot be simply treated as a constant when simulating the moisture diffusion, and Eq. (11) should be used as the governing equation. However, it should be noticed that there is one special condition: when C_{sat1}/C_{sat2} remains constant during dynamic thermal loading, the "standard method" is still valid.

2.3. Issues in diffusion analyses using ANSYS

Since the release of Version 14, ANSYS has started to support the diffusion analysis. The newly developed diffusion elements (Plane 238 and Solid 239) and couple field elements (Plane 223, Solid 226 and Solid 227) provide a convenient way to perform the moisture diffusion analysis and the thermal-structural-diffusion couple field analysis. Prior to Version 17, the temporal variation of C_{sat} or S in Eq. (11) will not be included in the calculation of the software [33]. Directly using a temperature-dependent C_{sat} for normalization will lead to erroneous results in the moisture diffusion analysis. In this paper, this method is called "conventional normalization approach". The root cause for the problem is discussed as follows:

The finite element expression for diffusion can be described as [34]

$$\left[K^d\right]\{C_e\} + \left[C^d\right]\left\{\dot{C}_e\right\} = \{R_e\} \tag{13}$$

where $\{C_e\}$ is the nodal concentration vector, $\{\dot{C}_e\}$ is the derivative of nodal concentration vector with respect to time, $[K^d]$ is the diffusion conductivity matrix, $[C^d]$ is the diffusion damping matrix, and $\{R_e\}$ represents the combination of the applied flow rate, the element diffusion flux, and the generation of diffusion substances.

As shown in the ANSYS theory manual [35], the diffusion conductivity matrix can be written as

$$\left[K^d\right] = C_{sat}\int_V \left(\nabla\{N\}^T\right)^T [D]\left(\nabla\{N\}^T\right) dV \tag{14}$$

In addition, the element diffusion damping matrix is

$$\left[C^d\right] = C_{sat}\int_V \{N\}\{N\}^T dV \tag{15}$$

where V is the element volume, $\{N\}$ is the shape function vector, and C_{sat} is the material property which can be input as the saturated concentration or solubility if the normalized concentration is used. When C_{sat} is not specified in the software, it defaults to be 1 and the actual moisture concentration is the field variable.

The above expression for $[K^d]$ in Eq. (14) is correct when C_{sat} does not change with time. Once C_{sat} is time-dependent, Eq. (14) is no longer valid, and the expression for $[K^d]$ becomes

$$\left[K^d\right] = C_{sat}\int_V \left(\nabla\{N\}^T\right)^T [D]\left(\nabla\{N\}^T\right) dV + \dot{C}_{sat}\int_V \{N\}^T\{N\} dV \tag{16}$$

where $\dot{C}_{sat}$ represents the varying rate of C_{sat}. Compared to Eq. (14), Eq. (16) has an additional term that is not considered in the ANSYS program of earlier versions. This is the fundamental reason why erroneous results will be yielded when C_{sat} is directly input as a temperature-dependent material property in the ANSYS software prior to Version 17. The same issue can also be found in several other commercial finite element software such as ABAQUS and COMSOL.

The release of ANSYS 17 offers a new solution to solving this issue. In the theory manual of ANSYS 17, it clearly states that C_{sat} can be input as a temperature-dependent material property and the temporal effect of C_{sat} will be numerically evaluated by the program during the analysis, which means the second term on the right-hand side in Eq. (16) is considered in the ANSYS 17. It should be noted that this new function can only be implemented using the couple field elements (Plane 223, Solid 226 and Solid 227) while it is not supported in the diffusion elements (Plane 238 and Solid 239) [36]. The validity of this new feature will be examined in this paper.

3. Overview of diffusion modeling

Researchers have proposed several different multi-material diffusion modeling techniques. In this section, the performance of each method in modeling diffusion under dynamic temperature condition is evaluated. The dynamic thermal loadings are classified into three different conditions in this paper: (1) Temperature changes with time and has spatially uniform distribution, but C_{sat1}/C_{sat2} keeps constant; (2) Temperature changes with time and has spatially uniform distribution, and C_{sat1}/C_{sat2} varies with time; (3) Temperature changes with time and has spatially non-uniform distribution. The applicability of different diffusion models towards three thermal loading conditions are discussed as follows.

3.1. The advanced normalization approach

To cope with the inherent limitation of the conventional normalization approach, Jang [37] proposed a method called "advanced normalization approach". This approach is based on the discovery that C_{sat} of most polymers depends weakly on the temperature, and has a linear relationship with the relative humidity. C_{sat} can be described with the following equation:

$$C_{sat} = SP_{ext} = S \times P_{sat} \times RH \tag{17}$$

Here, S is the solubility, P_{ext} is the ambient vapor pressure, P_{sat} is the saturated vapor pressure, and RH is the relative humidity. S and P_{sat} follow the Arrhenius relationship

$$S = S_0 \exp\left(\frac{E_s}{RT}\right) \tag{18}$$

$$P_{sat} = P_0 \exp\left(-\frac{E_{VP}}{RT}\right) \tag{19}$$

where S_0 and P_0 are the pre-exponential factors, E_S and E_{VP} are the activation energies for the solubility and the vapor pressure, respectively, and R is the universal gas constant 8.3145 J K^{-1} mol^{-1}. Combining Eqs. (17), (18) and (19), we can obtain the following relationship:

$$C_{sat} = S_0P_0 \exp\left(\frac{E_s - E_{VP}}{RT}\right) \times RH \tag{20}$$

It has been confirmed that, $E_S \approx E_{VP}$ [16] for most polymer-based electronic packaging materials. Thus, the exponential term in Eq. (20) is approximately equal to 1 and C_{sat} can be simplified as

$$C_{sat} \approx S_0 \times P_0 \times RH = M \times RH \tag{21}$$

Jang introduced the modified solubility M, which is a temperature-invariant parameter. M can be written in the following expression:

$$M = S_0P_0 \tag{22}$$

The new normalized concentration φ is defined as

$$\varphi = \frac{C}{M} \tag{23}$$

At the bi-material interface, the ratio of normalized concentrations for two materials is given by

$$\frac{\varphi_2}{\varphi_1} = \frac{S_2P/M_2}{S_1P/M_1} = \frac{S_2M_1}{S_1M_2} = \frac{S_{02}\exp\left(\frac{E_{S_2}}{RT}\right)S_{01}P_0}{S_{01}\exp\left(\frac{E_{S_1}}{RT}\right)S_{02}P_0} = \exp\left(\frac{E_{S_2} - E_{S_1}}{RT}\right) \tag{24}$$

The exponential term on the right-hand side in Eq. (24) equals 1 only if $E_{S1} = E_{S2}$. Therefore, in order to satisfy the continuity condition

at the material interface, the advanced normalization approach requires the equivalence between the activation energies of solubility for two materials. Because M is a constant, there is no additional term in the governing equation when applying the advanced normalization approach, and the governing equation can be written as

$$\frac{\partial \varphi}{\partial t} = D\left(\frac{\partial^2 \varphi}{\partial x^2} + \frac{\partial^2 \varphi}{\partial y^2} + \frac{\partial^2 \varphi}{\partial z^2}\right) \tag{25}$$

The advanced normalization approach is easy to perform in the finite element software and it is time efficient in the simulation. The only critical requirement is the approximate equivalence between activation energies of solubility for two materials, and this method works quite well if the required condition is fulfilled [37]. However, such approximation is not universally applicable. In essence, the advanced normalization approach is only a special condition of the standard method. It can only be applied under the thermal loading condition (1). Hence, this approach has a relatively limited field of application, and it may not be proper to be used in simulating the moisture diffusion in electronic devices under solder reflow.

3.2. The direct concentration approach

To overcome the challenges in moisture diffusion modeling under varying ambient temperature conditions, Xie et al. [38] proposed the direct concentration approach (DCA), which does not rely on the temperature-independence of C_{sat}. The DCA uses the moisture concentration C directly as the field variable instead of using the normalized concentration. To implement the DCA, two separate sets of coincident nodes need to be generated at the bi-material interface (Fig. 3). A set of constraint equations is applied at the interfacial nodes to establish the relationship between the moisture concentrations of two materials. The constraint equation is given by Eq. (26) as

$$\frac{C_1}{S_1} = \frac{C_2}{S_2} \tag{26}$$

where C_1 is the moisture concentration at interface on Material 1 side, and C_2 is the moisture concentration at interface on Material 2 side. We can find the form of Eq. (26) is similar to Eq. (4).

The DCA has been implemented using ABAQUS to study the moisture-related issues during the solder reflow [39]. Because the solubility is a function of temperature, constraint equations need to be updated at the time step where temperature changes over time. Under such circumstances, a new analysis with updated constraint equations should be performed when necessary. However, updating constraint equations during the computing process requires complicated subroutines. Moreover, it is difficult to apply the constraint equations when dealing with complicated 3-D models.

This approach appears to be correct by intuition. However, our study has shown that using the DCA will lead to the discontinuity of diffusion flux at the bi-material interface [40]

$$D_1 \frac{\partial C_1}{\partial n} \neq D_2 \frac{\partial C_2}{\partial n} \tag{27}$$

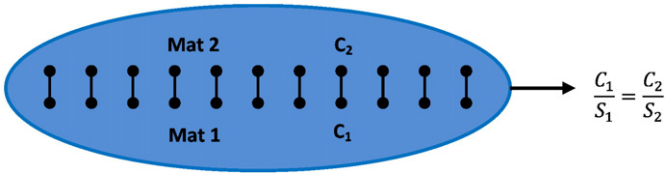

Fig. 3. Coincident nodes and constraint equations at bi-material interface.

where D_1 and D_2 are the diffusivities of Material 1 and Material 2, respectively, and n is the normal direction of the bi-material interface. Ref. [40] provides the proof of flux discontinuity under transient diffusion, which may not be straightforward enough. In this section, a more concise proof of flux discontinuity under steady state diffusion is illustrated.

To prove the flaw of DCA, one-dimensional (1-D) steady-state diffusion in a bi-material model is considered (Fig. 4). First-type boundary conditions (constant moisture concentrations) are applied at the material outside boundaries, and the initial concentration in two materials is zero. The ratio of saturated moisture concentration of the two materials ($\chi = C_{sat1}/C_{sat2}$) is a constant. Each material has two elements and three nodes, and the element size equals L. Two coincident nodes (Node 3 and Node 4) at the bi-material interface are generated for implementing the DCA.

For a steady state diffusion, the finite element governing equation can be expressed as

$$\left[K^d\right]\{C_e\} = \{R_e\} \tag{28}$$

The local conductivity matrix $[K^d]$ can be written as

$$\left[K^d\right] = \frac{D}{L}\begin{bmatrix} 1 & -1 \\ -1 & 1 \end{bmatrix} \tag{29}$$

Therefore, the global diffusion conductivity matrix becomes the following form after the assembly process:

$$\left[K^d\right] = \frac{1}{L}\begin{bmatrix} D_1 & -D_1 & 0 & 0 & 0 & 0 \\ -D_1 & 2D_1 & -D_1 & 0 & 0 & 0 \\ 0 & -D_1 & D_1 & 0 & 0 & 0 \\ 0 & 0 & 0 & D_2 & -D_2 & 0 \\ 0 & 0 & 0 & -D_2 & 2D_2 & -D_2 \\ 0 & 0 & 0 & 0 & -D_2 & D_2 \end{bmatrix} \tag{30}$$

As for $\{R_e\}$, the boundary condition is applied at Node 1 and Node 6, so $\{R_e\} = \{R_1, 0, 0, 0, 0, R_6\}^T$. In the DCA, the constraint equation is applied at interface nodes as

$$C_3 = \chi C_4 \tag{31}$$

To apply the boundary condition at the material interface using constraint equation, the master-slave elimination method is used. The degree-of-freedom (DOF) to be eliminated is called slave DOF, while the remaining one is the master DOF. After applying the constraint equation, a new set of DOFs $\{\overline{C_e}\}$ can be obtained. The relationship between $\{\overline{C_e}\}$ and $\{C_e\}$ can be established with the following transformation matrix $[T]$:

$$\{C_e\} = [T]\left\{\overline{C_e}\right\} \tag{32}$$

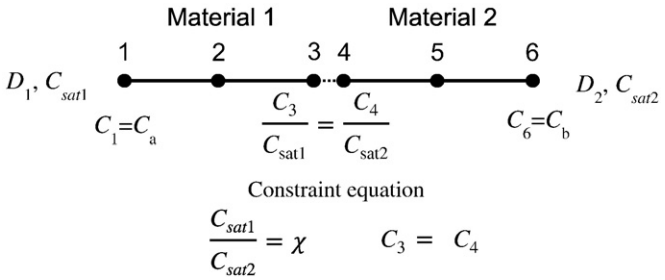

Fig. 4. One-dimensional diffusion in bi-material.

In this case, C_3 is treated as the slave DOF and C_4 is treated as the master DOF. Eq. (32) can be written in the full expression as follows:

$$\begin{Bmatrix} C_1 \\ C_2 \\ C_3 \\ C_4 \\ C_5 \\ C_6 \end{Bmatrix} = \begin{bmatrix} 1 & 0 & 0 & 0 & 0 \\ 0 & 1 & 0 & 0 & 0 \\ 0 & 0 & \chi & 0 & 0 \\ 0 & 0 & 1 & 0 & 0 \\ 0 & 0 & 0 & 1 & 0 \\ 0 & 0 & 0 & 0 & 1 \end{bmatrix} \begin{Bmatrix} C_1 \\ C_2 \\ C_4 \\ C_5 \\ C_6 \end{Bmatrix} \tag{33}$$

Plugging Eq. (32) into Eq. (28), and multiplying the equation by $[T]^T$ on both sides yields

$$[T]^T \left[K^d\right][T]\left\{\overline{C_e}\right\} = [T]^T\{R_e\} \tag{34}$$

Defining $[\overline{K^d}] = [T]^T[K^d][T]$ and $[\overline{R_e}] = [T]^T\{R_e\}$, Eq. (34) becomes

$$\left[\overline{K^d}\right]\left\{\overline{C^e}\right\} = \{R_e\} \tag{35}$$

The vector $\{R_e\}$ becomes $\{\overline{R_e}\} = \{R_1 \ 0 \ 0 \ 0 \ R_6\}^T$ after transformation. Applying the boundary conditions on Nodes 1 and 6, the new governing equation can be expressed as

$$\frac{1}{L}\begin{bmatrix} D_1 & -D_1 & 0 & 0 & 0 \\ -D_1 & 2D_1 & -\chi D_1 & 0 & 0 \\ 0 & -\chi D_1 & \chi^2 D_1 + D_2 & -D_2 & 0 \\ 0 & 0 & -D_2 & 2D_2 & -D_2 \\ 0 & 0 & 0 & -D_2 & D_2 \end{bmatrix} \begin{Bmatrix} C_a \\ C_2 \\ C_4 \\ C_5 \\ C_b \end{Bmatrix} = \begin{Bmatrix} R_1 \\ 0 \\ 0 \\ 0 \\ R_6 \end{Bmatrix} \tag{36}$$

Considering only the third row, expanding the equation and re-arranging the items yields

$$\chi\frac{D_1(\chi C_4 - C_2)}{L} = \frac{D_2(C_5 - C_4)}{L} \tag{37}$$

Because $\chi C_4 = C_3$, the above equation can be rewritten as

$$\chi\frac{D_1(C_3 - C_2)}{L} = \frac{D_2(C_5 - C_4)}{L} \tag{38}$$

The left-hand side of Eq. (38) is the diffusion flux J_1 at the interface on Material 1 side, and the right-hand side is equal to the diffusion flux J_2 at the interface on Material 2 side. Because $\chi \neq 1$ for bi-material, the above relationship $\chi J_1 = J_2$ cannot satisfy the diffusion flux continuity condition at the material interface, which means the DCA violates the law of mass conservation. It is only valid when the diffusion flux across the material interface is negligible ($J_1 \approx J_2 \approx 0$). Using the DCA directly in simulating moisture diffusion in IC packages during solder reflow can result in unexpected errors.

3.3. The peridynamic approach

The peridynamic theory is a nonlocal continuum theory, which was introduced by Silling [41] to overcome the difficulties in the structural analysis due to the existence of discontinuity. In the peridynamic theory, the state of a material point is influenced by the other material points located within a domain $\Re$ (Fig. 5). The peridynamic governing equation can be expressed as

$$\rho\ddot{u}(x,t) = \int_{\Re} f(u(x',t) - u(x,t), x' - x)dV_{x'} + b(x,t) \tag{39}$$

where u is the displacement, ρ is the density, b is the body force, V is the volume of a material point and f is the response function that describes the interaction between material points x and x'.

The peridynamic theory is based on the integral-formed governing equations rather than the partial differential equations that classical continuum theory uses. Because the integral based governing equations remain valid in the presence of discontinuities, it removes the requirement to impose continuity conditions at the material interfaces. Thus, it may fundamentally solve the problems with discontinuities, such as moisture diffusion in a multi-material system. Oterkus et al. [43] has applied the peridynamic theory in the moisture diffusion and hygro-thermo-mechanical stress analyses in electronic packages. The peridynamic governing equation for diffusion can be written as

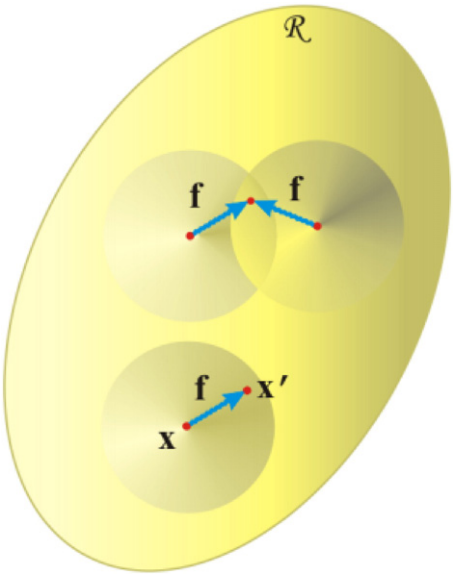

Fig. 5. Interaction between material points within a domain $\Re$ [42].

$$\frac{\partial C(x,t)}{\partial t} = \int_{\Re} f_c\left(C(x,t), C'(x',t), x, x', t\right)dV_{x'} \tag{40}$$

where f_c is the diffusion response function and can be expressed as

$$f_c(x', x, t) = d\frac{C(x',t) - C(x,t)}{|x' - x|} \tag{41}$$

d is defined in terms of the diffusivity D as

$$d = \frac{2D}{A\delta^2} \text{ for 1-D } d = \frac{6D}{\pi h\delta^2} \text{ for 2-D } d = \frac{6D}{\pi h\delta^4} \text{ for 3-D} \tag{42}$$

where A is the cross-sectional area, h is the thickness and δ is the size of domain $\Re$.

The peridynamic technique is totally different from the finite element method, and it has the potential to overcome the difficulty in simulating the moisture diffusion during reflow. However, such a method usually requires specially written meshless code. There is no commercially available peridynamic software, which restricts its field of application. Han et al. [44] applied the peridynamic theory in the finite element software ANSYS for simulating moisture diffusion and named this method as "Peridynamic direct concentration approach". Similar with the DCA, the concentration is directly used as the field variable in this approach. To combine the peridynamic theory with ANSYS, the thermal mass element (Mass 71) and thermal link element (Link 33) can be used to model the material points and the peridynamic bonds, respectively. The diffusivities can be assigned as the volume (V) of material points for the material property input and the cross-sectional area A of the link element can be expressed as $A = Vd$ for the real constant input. In the simulation, the diffusivity at the material interface needs special treatment. For example, the diffusivity D_m between two material points

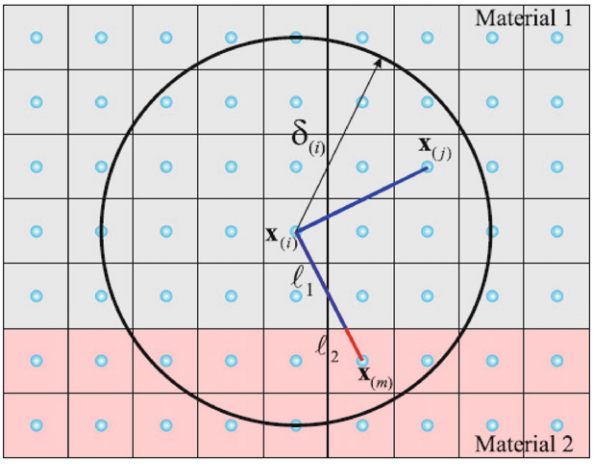

Fig. 6. Interaction between material points at the material interface [45].

across the material interface (as shown in Fig. 6) can be calculated as

$$D_m = \frac{l_1 + l_2}{\frac{l_1}{D_1} + \frac{l_2}{D_2}} \tag{43}$$

where l_1 and l_2 represent the segments of peridynamic bond in Materials 1 and 2, respectively, and D_1 and D_2 are the diffusivities of Materials 1 and 2, respectively.

This peridynamic direct concentration approach appears to be correct at the first glance. However, in the case study of Ref. [44], the obtained moisture concentration across the multi-material interface is continuous, which is not conformed to the basic assumption of the concentration discontinuity at the material interface. It is not difficult to imagine the root cause of the continuous concentration results. Because the peridynamic direct concentration approach utilizes the thermal diffusion module in ANSYS, the temperature will always be continuous at the material interface. A "peridynamic normalized concentration approach" is needed to generate the concentration discontinuity at the material interface. The governing equation for the peridynamic normalized concentration approach can be easily obtained by modifying Eq. (40) as

$$\frac{\partial(C_{sat} w(x,t))}{\partial t} = \int_{\mathcal{H}} f_w(w(x,t), w'(x',t), x, x', t) dV_{x'} \tag{44}$$

The response function can be expressed as

$$f_w\left(x', x, t\right) = dC_{sat} \frac{w(x',t) - w(x,t)}{|x' - x|} \tag{45}$$

Although "peridynamic normalized concentration approach" can solve the concentration discontinuity problem, the geometry modeling with the thermal link and thermal mass elements is complicated and time-consuming when dealing with 2-D or 3-D models in ANSYS. It should also be noticed that the left-hand side of Eq. (44) is similar to Eq. (11), which means it cannot be directly implemented in ANSYS under a dynamic thermal loading condition for the similar reason to the conventional normalization approach.

3.4. The piecewise normalization approach

Assuming mass conservation, Wong [46,47] introduced an advanced diffusion modeling technique named "piecewise normalization approach". Zhu et al. [48] and Ikeda et al. [49] also applied this approach in modeling the moisture diffusion in a multi-material system. To implement this approach, the transient diffusion analysis will be cut into a set of piecewise load steps. The continuity of the moisture concentration between load steps should be satisfied based on the mass conservation. At the beginning of each load step, the initial wetness field needs to be updated based on the wetness field from the previous load step as shown in Fig. 7.

The advantage of this approach is that the concentration continuity condition at the material interface for each load step is automatically satisfied. Besides, it provides a way to simulate the moisture diffusion under more general transient thermal loading conditions. The pricewise normalization approach can be applied under thermal loading conditions (1) and (2). However, it is not implementable in the thermal loading condition (3). Moreover, the calculation time for this method is quite long due to sophisticated subroutines and multiple time steps. The size of time step is crucial to ensure accuracy. The selection of the time step size used in the analysis should be based on the rate of temperature change. The higher the rate, the smaller time step size is needed. Theoretically, the numerical solution will converge to an exact solution when the time step size is small enough in the calculation.

3.5. The internal source approach

Wong [50] introduced an alternative method called "internal source approach", which aimed to solve moisture diffusion problems under a transient thermal loading condition. In this paper, this method is clarified and re-expressed in a purely mathematical way. This method utilizes the function of applying the internal source boundary condition to compensate for the term in Eq. (11), which is omitted by the FEA software.

If there is an internal diffusion generation source in a material, the diffusion governing equation should be written as

$$\frac{\partial C}{\partial t} = D\left(\frac{\partial^2 C}{\partial x^2} + \frac{\partial^2 C}{\partial y^2} + \frac{\partial^2 C}{\partial z^2}\right) + r \tag{46}$$

where r is the internal diffusion generation source. Substituting $C = wC_{sat}$ into Eq. (46) and rearranging the equation gives

$$\frac{\partial w}{\partial t} = D\left(\frac{\partial^2 w}{\partial x^2} + \frac{\partial^2 w}{\partial y^2} + \frac{\partial^2 w}{\partial z^2}\right) + \frac{r}{C_{sat}} \tag{47}$$

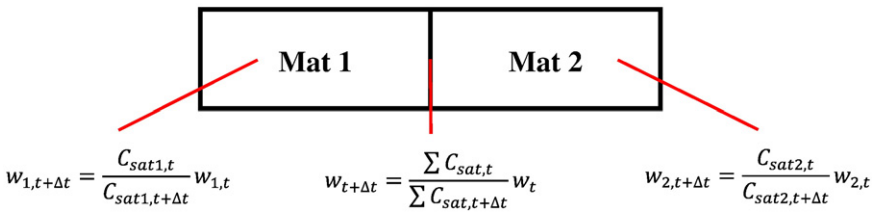

Fig. 7. Boundary conditions for piecewise normalization approach.

Moving the second term of Eq. (11) from the left-hand side to the right-hand side yields

$$\frac{\partial w}{\partial t} = D\left(\frac{\partial^2 w}{\partial x^2} + \frac{\partial^2 w}{\partial y^2} + \frac{\partial^2 w}{\partial z^2}\right) + \frac{w}{C_{sat}}\frac{\partial C_{sat}}{\partial t} \tag{48}$$

Assuming Eqs. (47) and (48) are equal, the following expression can be obtained:

$$r = -w\frac{\partial C_{sat}}{\partial t} \tag{49}$$

Mathematically, the internal source term in Eq. (47) can be used to represent the last term on the right-hand side in Eq. (48). Assuming the wetness field w_{t_i} at a given time t_i is known, and the objective is to obtain the wetness field $w_{t_i+\Delta t}$ at time $t_i+\Delta t$. The saturated moisture concentrations at t_i and $t_i+\Delta t$ are $C_{sat}^{t_i}$ and $C_{sat}^{t_i+\Delta t}$, respectively. The derivative term in Eq. (49) can be expressed in the finite difference form as

$$r = -w\frac{\partial C_{sat}}{\partial t} = -w_{t_i+\Delta t}\frac{C_{sat}^{t_i+\Delta t} - C_{sat}^{t_i}}{\Delta t} = w_{t_i+\Delta t}\frac{C_{sat}^{t_i} - C_{sat}^{t_i+\Delta t}}{\Delta t} \tag{50}$$

Thus, Eq. (47) can be rewritten as

$$\frac{\partial w_{t_i+\Delta t}}{\partial t} = D\left(\frac{\partial^2 w_{t_i+\Delta t}}{\partial x^2} + \frac{\partial^2 w_{t_i+\Delta t}}{\partial y^2} + \frac{\partial^2 w_{t_i+\Delta t}}{\partial z^2}\right) + \frac{w_{t_i+\Delta t}}{C_{sat}^{t_i+\Delta t}}\frac{C_{sat}^{t_i} - C_{sat}^{t_i+\Delta t}}{\Delta t} \tag{51}$$

In order to implement the internal source approach, the value of r first needs to be calculated. In Eq. (50), $w_{t_i+\Delta t}$ is an undetermined term and cannot be used to determine r. Within a relatively small time increment Δt, there will be negligible change in moisture concentration. Hence, in order to perform the analysis, $w_{t_i+\Delta t}$ can be expressed in terms of w_{t_i} based on the mass conservation:

$$w_{t_i}C_{sat}^{t_i} = w_{t_i+\Delta t}C_{sat}^{t_i+\Delta t} \tag{52}$$

In this way, the internal source term r can be applied as a boundary condition to compensate for the derivative term omitted by the FEA software.

$$\frac{\partial w_{t_i+\Delta t}}{\partial t} = D\left(\frac{\partial^2 w_{t_i+\Delta t}}{\partial x^2} + \frac{\partial^2 w_{t_i+\Delta t}}{\partial y^2} + \frac{\partial^2 w_{t_i+\Delta t}}{\partial z^2}\right) + w_{t_i}\frac{C_{sat}^{t_i}}{\left(C_{sat}^{t_i+\Delta t}\right)^2}\frac{C_{sat}^{t_i} - C_{sat}^{t_i+\Delta t}}{\Delta t} \tag{53}$$

Alternatively, the above equation can also be expressed using another normalized concentration ϕ and solubility S as

$$\frac{\partial \phi_{t_i+\Delta t}}{\partial t} = D\left(\frac{\partial^2 \phi_{t_i+\Delta t}}{\partial x^2} + \frac{\partial^2 \phi_{t_i+\Delta t}}{\partial y^2} + \frac{\partial^2 \phi_{t_i+\Delta t}}{\partial z^2}\right) + \phi_{t_i}\frac{S^{t_i}}{\left(S^{t_i+\Delta t}\right)^2}\frac{S^{t_i} - S^{t_i+\Delta t}}{\Delta t} \tag{54}$$

The procedure for the implementation of the internal source approach is illustrated in Fig. 8. First, the saturated moisture concentration C_{sat} or the solubility S should be input as a temperature-dependent material property in the FEA software so as to be updated at each incremental time step. At time t_i, the normalized concentration field needs first to be obtained to determine the value of internal source term r_i. Then, r_i should be applied as the boundary condition in the next time step in order to calculate the normalized concentration field at time $t_i+\Delta t$. Because the concentration field needs to be read in the postprocessor after the completed solution at each time step, a restart analysis needs to be used in the following time step, which adds additional calculation time.

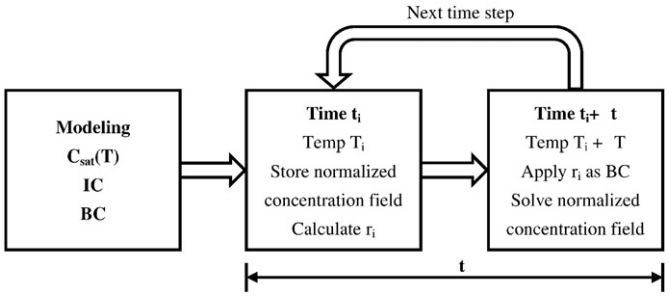

Fig. 8. Flow chart for implementation of the internal source approach.

The internal source approach is a promising method because there is no specific restriction on this method and it can satisfy all three dynamic thermal loading conditions. However, one shortcoming of this approach is that the intensive restarts during the simulation make the calculation time-consuming. The other shortcoming is that theoretical error exists due to the approximate equivalence of w_{t_i} and $w_{t_i+\Delta t}$. There are two ways to minimize such errors. One straightforward way is reducing the time step size Δt. The other way is to perform the simulation twice. After the first-time calculation, $w_{t_i+\Delta t}$ at each time step can be obtained. Then $w_{t_i+\Delta t}$ will be applied as the boundary instead of the expression using w_{t_i} in the second-time calculation. In this way, a relatively accurate result can be obtained.

4. Case studies

To examine the feasibility and accuracy of different approaches in solving diffusion problems, case studies were performed with both ANSYS 15 and ANSYS 17. The case study considered a one-dimensional (1-D) desorption process in a bi-material system under a varying temperature condition. The geometry of the model is shown in Fig. 9 and material properties are listed in Table 1.

The bi-material system was assumed to be fully saturated at an initial state of 85 °C/100% RH. To simulate the desorption process, the concentrations of the leftmost and rightmost boundaries were set as zero. In the first case, the temperature in the system was spatially uniform, but temporally varied as $T(t) = (85 + 2t)^{\circ}$C. C_{sat} changed with temperature and could be calculated with Eq. (20). The ratio of saturated moisture concentrations of two materials (C_{sat1}/C_{sat2}) remained a constant value during the entire calculation. The diffusion element Plane 238 was used for the finite element simulation in ANSYS 15, while the couple-field element Plane 226 was used in the simulation in ANSYS 17.

Choosing a proper time step size is crucial for the transient diffusion analysis that uses the finite element method. Too small a time step may excite oscillations in the solution, while too large a time step may result in inaccurate results especially near the material interfaces. ANSYS theory manual [35] suggests that the time step Δt should follow

$$\Delta t \geq \frac{\Delta L^2}{4D} \tag{55}$$

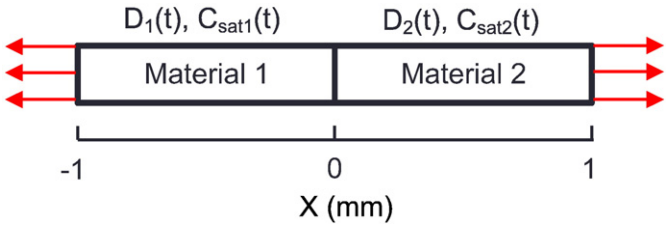

Fig. 9. Geometry and boundary conditions for the case study.

Table 1
Moisture material properties used in the simulation.

	Material 1	Material 2
D_0 ($m^2\ s^{-1}$)	5×10^{-3}	4×10^{-3}
S_0 ($kg\ m^{-3}\ Pa^{-1}$)	6×10^{-10}	2×10^{-10}
E_D ($J\ mol^{-1}$)	5×10^{4}	5×10^{4}
E_S ($J\ mol^{-1}$)	4×10^{4}	4×10^{4}
P_0 (Pa)	5.0492×10^{10}	5.0492×10^{10}
E_{VP} ($J\ mol^{-1}$)	4.0873×10^{4}	4.0873×10^{4}

where ΔL is the characteristic element length and D is the diffusivity. In this study, the time step Δt was chosen as 2 s.

In this case study, six different methods were compared: (1) the internal source approach (ISA); (2) the piecewise normalization approach; (3) the advanced normalization approach; (4) the conventional normalization approach with ANSYS 15; (5) the conventional normalization approach with ANSYS 17; and (6) the direct concentration approach (DCA). Except for (5), which was performed in ANSYS 17, all other methods were implemented in ANSYS 15. For the conventional normalization approach, C_{sat} was directly input as a temperature-dependent material property in ANSYS, which means a varying C_{sat} was used in the normalized variable.

To verify the accuracy of the diffusion results from different methods, a numerical solution based on the finite difference method (FDM) was used as the reference. For this one-dimensional diffusion problem, the governing equation can be written as

$$C_{sat}\frac{\partial w}{\partial t}+w\frac{\partial C_{sat}}{\partial t}-DC_{sat}\frac{\partial^2 w}{\partial x^2}=0 \tag{56}$$

Applying the forward difference in the first term and central difference in the third term [28], Eq. (56) becomes

$$C_{sat}^{t}\frac{w_x^{t+\Delta t}-w_x^{t}}{\Delta t}+w_x^{t}\dot{C}_{sat}^{t}-D^{t}C_{sat}^{t}\frac{w_{x+\Delta x}^{t}-2w_x^{t}+w_{x-\Delta x}^{t}}{\Delta x^2}=0 \tag{57}$$

The normalized concentration $w_x^{t+\Delta t}$ can be expressed as

$$w_x^{t+\Delta t}=\frac{D^{t}\Delta t}{\Delta x^2}w_{x+\Delta x}^{t}+\left(1-2\frac{D^{t}\Delta t}{\Delta x^2}-\frac{\dot{C}_{sat}^{t}}{C_{sat}^{t}}\Delta t\right)w_x^{t}+\frac{D^{t}\Delta t}{\Delta x^2}w_{x-\Delta x}^{t} \tag{58}$$

At the material interface, the diffusion flux continuity should be satisfied as follows:

$$D_1C_{sat1}\left.\frac{\partial w}{\partial x}\right|_{L-}=D_2C_{sat2}\left.\frac{\partial w}{\partial x}\right|_{L+} \tag{59}$$

where the subscript $L-$ and $L+$ represents the Material 1 side and Material 2 side at the interface L. Then, the normalized concentration w_L at the material interface can be expressed as

$$w_L^{t}=\frac{D_1^{t}C_{sat1}^{t}w_{L-\Delta x}^{t}+D_2^{t}C_{sat2}^{t}w_{L+\Delta x}^{t}}{D_1^{t}C_{sat1}^{t}+D_2^{t}C_{sat2}^{t}} \tag{60}$$

Moisture concentration results at $t = 20$ s, 40 s, 60 s and 80 s were obtained for comparison, which are shown in Fig. 10. Except for the conventional normalization approach with ANSYS 15 and 17, as well as the direct concentration approach, which generates different results from the reference, all other techniques return almost identical results to

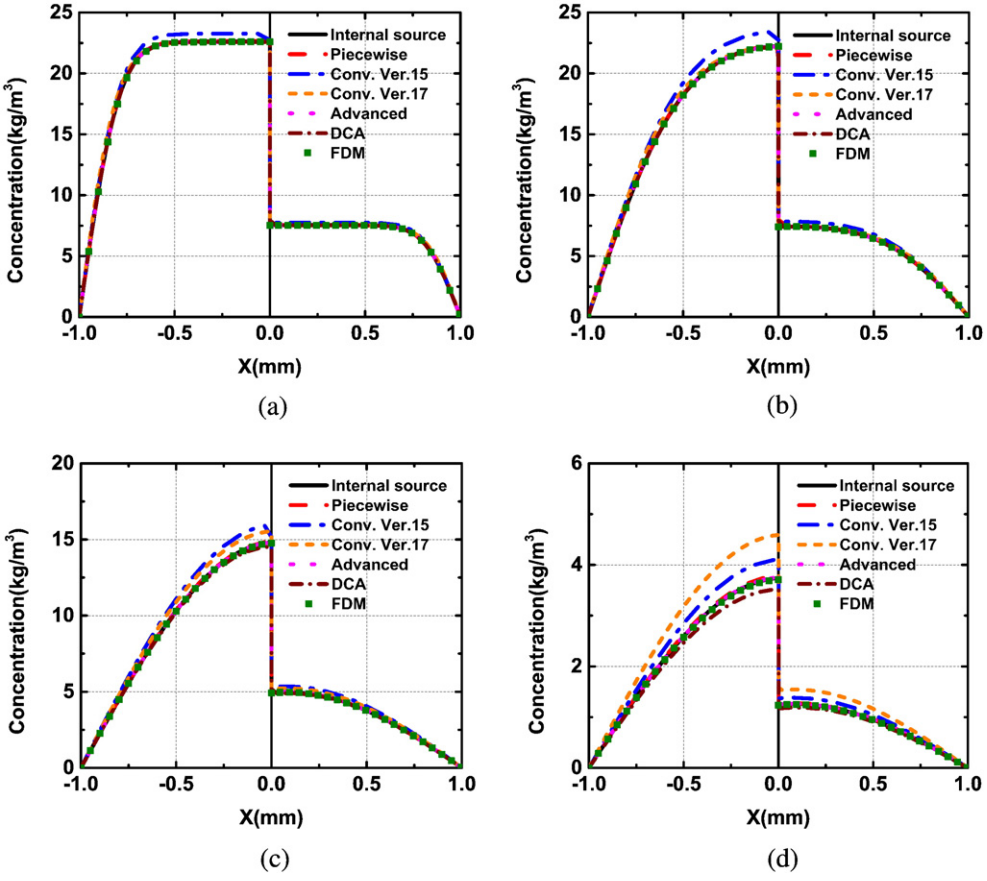

Fig. 10. Moisture concentration distributions in Case 1 (a) $t = 20$ s (b) $t = 40$ s (c) $t = 60$ s (d) $t = 80$ s.

the reference. For the conventional normalization approach using ANSYS 15, such a difference is caused by the finite element software itself because the effect of varying C_{sat} is not included in the calculation, which is conformed to the previous conclusion in Ref. [33]. The newest ANSYS 17 generates similar results to the reference at 20 s and 40 s while it yields higher results than the reference at 60 s and 80 s. The direct concentration approach produces slightly lower results than the reference at 80 s, but it works well at 20 s, 40 s and 60 s. The advanced normalization approach shows good performance in this case because the critical requirement $E_{S1} = E_{S2}$ is fulfilled, and it costs much less calculation time than the internal source approach and the piecewise normalization approach.

The above case study considered a special condition that C_{sat} changed with time, but the ratio of C_{sat} for two materials (C_{sat1}/C_{sat2}) remained constant. However, such a condition is not universal and it is not usually seen in the real world. Thus, a second case study was performed considering a more general condition. In the second case, only the activation energy of solubility (E_S) of Material 2 was changed to 4.5×10^4 J mol^{-1}, while all other conditions kept the same as in the first case. The ratio of saturated moisture concentrations of two materials (C_{sat1}/C_{sat2}) would vary with time in this case study.

The corresponding results of moisture concentration in Case 2 are plotted in Fig. 11. It is evident that only the internal source approach and the piecewise normalization approach produce similar moisture concentration results to the reference while other methods do not. The direct concentration approach yields slightly different results from reference and such difference can be visually seen at 60 s and 80 s. Unlike the performance in the previous case, the results from advanced normalization approach show a large deviation from reference in this case study. Because the activation energies of solubility for two materials are not identical, the critical requirement for utilizing the advanced normalization approach is not satisfied in this case. Therefore, applying this approach can result in incorrect results. The concentration discrepancy especially near the interface can cause significant errors when calculating the hygroscopic stress and the vapor pressure, thus affecting the accurate prediction for the interfacial delamination behavior. It is not surprising that the conventional normalization approach with ANSYS 15 leads again to a wrong result. For the conventional normalization approach with ANSYS 17, similar to the previous case, the results conform to the reference except for 60 s and 80 s.

Table 2
Thermal material properties.

	Material 1	Material 2
k (W m^{-1}K^{-1})	0.2	0.6
ρ (kg m^{-3})	3000	3000
c_p (J kg^{-1}K^{-1})	1500	1500

For a realistic dynamic thermal loading condition such as reflow, the temperature within the materials will change with time and distribute non-uniformly. A third case was performed considering the actual heat transfer process and the temperature gradient within the materials. The thermal material properties for Materials 1 and 2 are listed in Table 2. The moisture material properties are the same as Case 2. Varying temperature boundary condition was applied at only exteriors of Material 1 and Material 2. For such an anisothermal condition, the only methods that can be implemented are the internal source approach and the conventional normalization approach using ANSYS 17. The sequentially coupled thermal-diffusion analysis was performed to implement the internal source approach, while a direct coupling method was

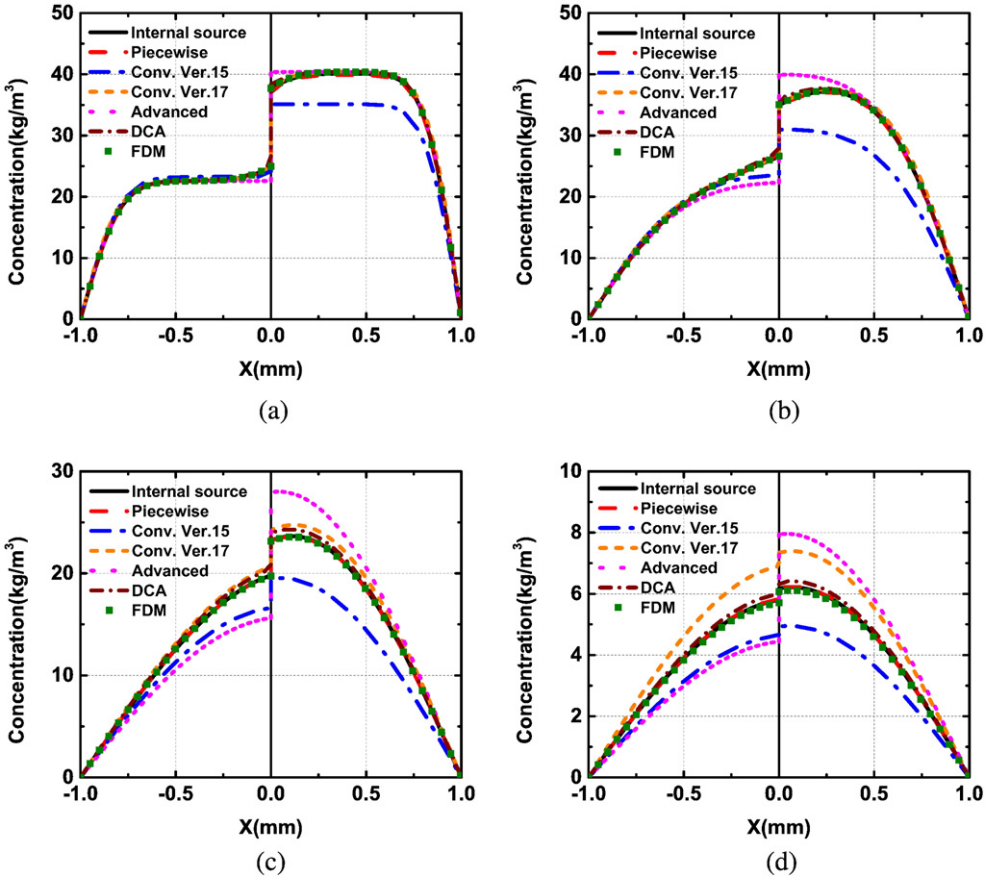

Fig. 11. Moisture concentration distributions in Case 2 (a) $t = 20$ s (b) $t = 40$ s (c) $t = 60$ s (d) $t = 80$ s.

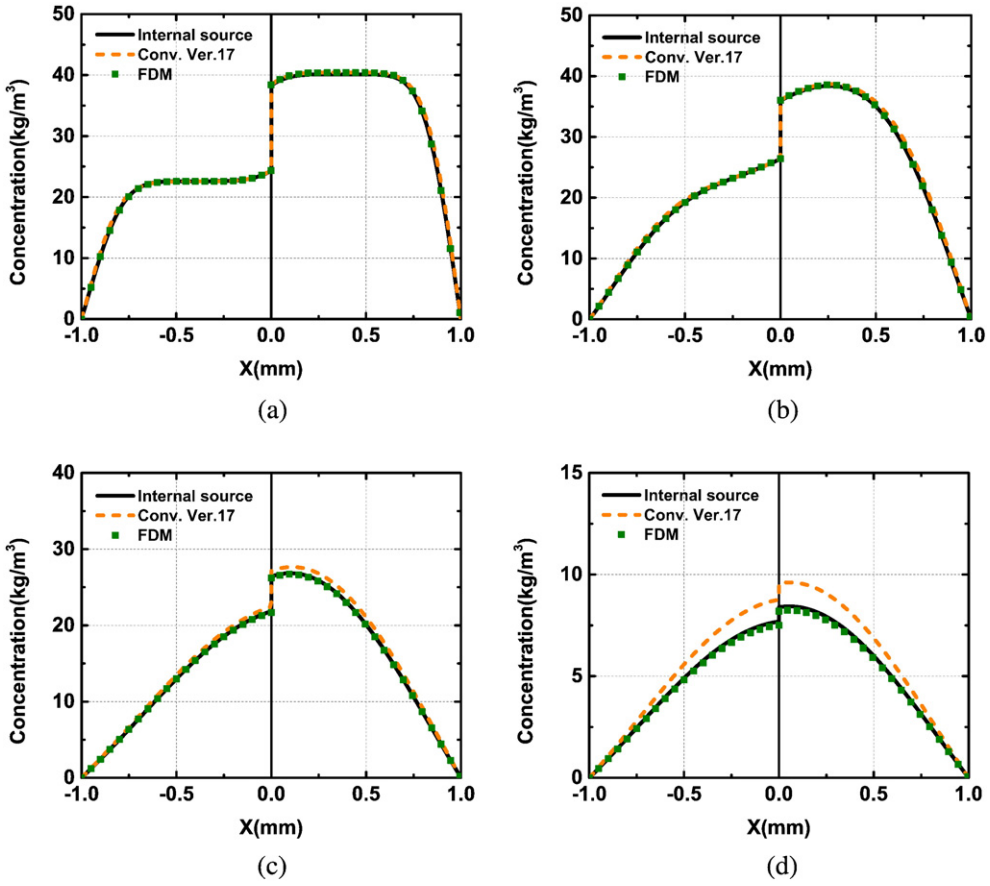

Fig. 12. Moisture concentration distributions in Case 3 (a) $t = 20$ s (b) $t = 40$ s (c) $t = 60$ s (d) $t = 80$ s.

used for the conventional normalization approach in ANSYS 17. Fig. 12 shows the moisture concentration results generated from the two methods. Again, the internal source approach yields similar results to the reference. The results produced by the conventional normalization approach using ANSYS 17 are slightly larger than the reference results at 60 s and 80 s.

5. Discussion

In the above three cases, the conventional normalization approach with ANSYS 17 generates slightly different results from the reference at 60 s and 80 s. Nonetheless, it does not mean ANSYS 17 cannot solve such diffusion problems correctly. A closer examination reveals that such an error results from the relatively large time step size (2 s). Fig.13 shows the concentration distribution at 80 s under different time step sizes for all three cases. It can be found that the result difference decreases as the time step size decreases. Although ANSYS 17 provides a convenient way to simulate the bi-material diffusion under transient thermal loadings with temperature-dependent C_{sat}, users should be careful in choosing a proper time step size during the simulation. For the case studies in this paper, although the calculation time of the internal source approach is long due to the multiple restarts, it yields more accurate results compared to the conventional normalization approach with ANSYS 17 under the same time step size. The internal source approach can accurately predict moisture concentration distributions in all three dynamic temperature loading conditions, which means it has potentially broader fields of application.

As for the direct concentration approach, its performance in Cases 1 and 2 can mislead people to think it is correct. The root cause of such a false impression is the approximation of Fourier numbers for Materials 1 and 2 ($Fo_1/Fo_2 = 1.25$). Fourier number Fo is defined as

$$Fo = \frac{Dt}{L^2} \tag{61}$$

where D is the diffusivity, t is the characteristic time and L is the characteristic length.

When the ratio of Fourier numbers between two adjacent materials (Fo_1/Fo_2) is close to 1, the diffusion flux across the material interface approaches 0. In this situation, the effect of flux discontinuity generated by the DCA will be minimized. A parametric study was performed to examine the influence of Fourier number ratio between two materials on the concentration result from DCA. In this case, temperature and moisture boundary condition are the same as in Case 1. Different Fourier number ratios were obtained by modifying the diffusivities of two materials. The concentration difference between the results from DCA and reference at the material interface on Material 1 side was calculated under different Fourier number ratios (Fo_1/Fo_2). It can be seen from Fig. 14, as the ratio of Fourier number between two materials (Fo_1/Fo_2) increases, the concentration difference between the results from DCA and reference increases. Such a difference is also affected by time. As time goes on, the concentration difference increases significantly. When the Fourier number ratio is less than 1.25, the difference between DCA and reference is in a small range (less than 6%). If a small error is permitted, the DCA can generate reasonable results when the Fourier number ratio between two materials is close to 1.

6. Summary

This paper summarized the critical challenges of moisture diffusion analysis in a multi-material system and addressed the fundamental

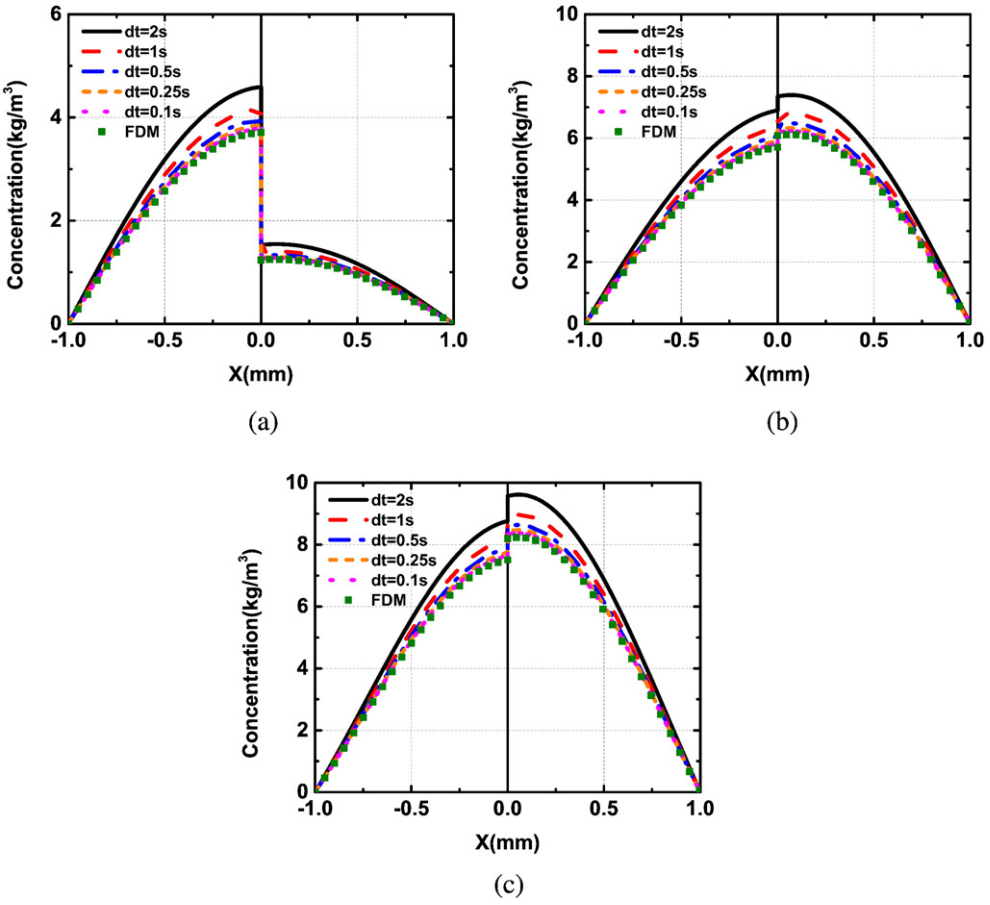

Fig. 13. Moisture concentration results at 80 s from ANSYS 17 with different time step size (a) Case 1 (b) Case 2 (c) Case 3.

reason why most commercial finite element software cannot directly solve the diffusion problem under a dynamic thermal loading condition with a temperature-dependent C_{sat}. Different diffusion modeling techniques were reviewed and analyzed. Case studies were performed to compare the results of different approaches under three different transient thermal loading conditions.

It was theoretically proved that the direct concentration approach cannot satisfy the diffusion flux continuity condition across the material interface. The direct concentration approach can only be applied when the diffusion flux across the material interface is approximately equal to 1. The peridynamic direct concentration approach cannot generate moisture concentration discontinuity at the material interface, while the peridynamic normalized concentration approach cannot be applied under dynamic thermal loading conditions when implemented in ANSYS. The piecewise normalization approach was shown to be effective when simulating moisture diffusion in a bi-material system under dynamic thermal loading conditions with uniform temperature distribution. The internal source approach was clarified and re-expressed in a purely mathematical way. The internal source approach was validated as a universal method in simulating moisture diffusion under all three types of dynamic thermal loading conditions. The new function of diffusion module in ANSYS 17 was examined and validated in case studies. It has been shown that the proper time step size selection is important to obtain accurate results in diffusion analysis with ANSYS 17.

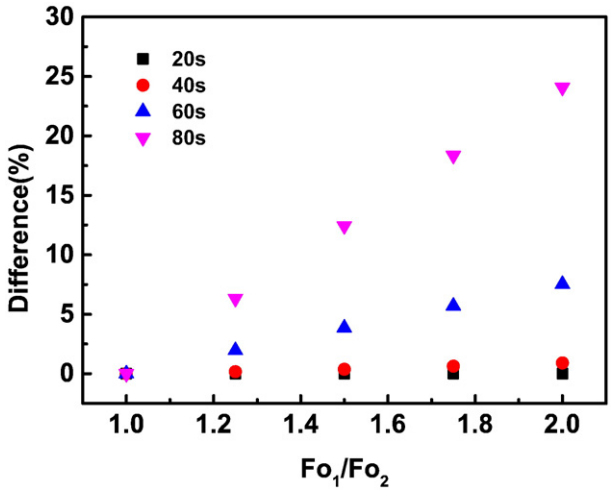

Fig. 14. Effect of Fourier number on the accuracy of DCA.

References

[1] M. Kitano, A. Nishimura, S. Kawai, Analysis of package cracking during reflow soldering process, 26th Int. Reliab. Phys. Sympo 1988, pp. 90–95.
[2] T. Ferguson, J. Qu, Effect of moisture on the interfacial adhesion of the underfill/solder mask interface, J. Electron. Packag. 124 (2) (2002) 106–110.
[3] E.H. Wong, R. Rajoo, S.W. Koh, T.B. Lim, The mechanics and impact of hygroscopic swelling of polymeric materials in electronic packaging, J. Electron. Packag. 124 (2) (2002) 122–126.
[4] X.J. Fan, G.Q. Zhang, W.D. Driel, L.J. Ernst, Interfacial delamination mechanisms during soldering reflow with moisture preconditioning, IEEE Trans. Comp. Packag. Technol. 31 (2) (2008) 252–259.
[5] X.J. Fan, Mechanics of moisture for polymers: fundamental concepts and model study, Proc. of 9th EuroSime 2008, pp. 159–172.
[6] S. Liu, Y. Mei, Behavior of delaminated plastic IC packages subjected to encapsulation, cooling, moisture absorption, and wave soldering, IEEE Trans. Compon. Packag. Manuf. Technol. A 18 (3) (1995) 634–645.
[7] T.Y. Tee, C.L. Kho, D. Yap, C. Toh, X. Baraton, Z. Zhong, Reliability assessment and hygroswelling modeling of FCBGA with no-flow underfil, Microelectron. Reliab. 43 (5) (2003) 741–749.
[8] J. Zhou, Sequentially-coupled finite element transient analysis with hygroscopic swelling, Proc. of 7th EuroSimE 2006, pp. 1–6.

[9] H.C. Hsu, Y.T. Hsu, Characterization of hygroscopic swelling and thermo-hygro-mechanical design on electronic package, J. Mech. 25 (03) (2009) 225–232.
[10] E. Parsa, H. Huang, A. Dasgupta, Multi-physics simulations for combined temperature/humidity loading of potted electronic assemblies, Microelectron. Reliab. 54 (6) (2014) 1182–1191.
[11] Y. Kim, D. Liu, H. Lee, R. Liu, D. Sengupta, S. Park, Investigation of stress in MEMS sensor device due to hygroscopic and viscoelastic behavior of molding compound, IEEE Trans. Compon. Packag. Manuf. Technol. 5 (7) (2015) 945–955.
[12] J.B. Kwak, S. Park, Integrated hygro-swelling and thermo-mechanical behavior of mold compound for MEMS package during reflow after moisture preconditioning, Microelectron. Int. 32 (1) (2015) 8–17.
[13] T.Y. Tee, X.J. Fan, T.B. Lim, Modeling of whole field vapor pressure during reflow for flip chip BGA and wire bond PBGA packages, Proc. of the First Electronics Material Packaging Workshop 1999, pp. 38–45.
[14] T.Y. Tee, Z. Zhong, Integrated vapor pressure, hygroswelling and thermo-mechanical stress modeling of QFN package during reflow, Microelectron. Reliab. 44 (1) (2004) 105–114.
[15] E.H. Wong, S.W. Koh, K.H. Lee, K. Lim, T. Lim, Y. Mai, Advances in vapor pressure modeling for electronic packaging, IEEE Trans. Adv. Packag. 29 (2006) 751–759.
[16] M. Zhang, S.W.R. Lee, A novel vapor pressure transfusion model for the popcorning analysis of Quad Flat No-lead (QFN) packages, 3rd Electron. Sys. Integ. Tech. Conf 2010, pp. 1–9.
[17] J. Wang, S. Park, Non-linear finite element analysis on stacked die package subjected to integrated vapor-hygro-thermal-mechanical stress, 66th Elect. Compon. Technol. Conf 2016, pp. 1394–1401.
[18] A.A.O. Tay, Modeling of interfacial delamination in plastic IC packages under hygrothermal loading, J. Electron. Packag. 127 (3) (2005) 268–275.
[19] A.A.O. Tay, T.Y. Lin, Influence of temperature, humidity, and defect location on delamination in plastic IC packages, IEEE Trans. Compon. Packag. Manuf. Technol. 22 (4) (1999) 512–518.
[20] A.A.O. Tay, K.Y. Goh, A study of delamination growth in the die-attach layer of plastic IC packages under hygrothermal loading during solder reflow, IEEE Trans. Dev. Mater. Reliab. 3 (4) (2003) 144–151.
[21] M.A.J. Van Gils, P. Habets, G.Q. Zhang, W.D. van Driel, P.J. Schreurs, Characterization and modelling of moisture driven interface failures, Microelectron. Reliab. 44 (9–11) (2004) 1317–1322.
[22] J.H. Lau, S.W.R. Lee, Temperature-dependent popcorning analysis of plastic ball grid array package during solder reflow with fracture mechanics method, J. Electron. Packag. 122 (1) (2000) 34–41.
[23] G. Hu, R. Rossi, J. Luan, X. Baraton, Interface delamination analysis of TQFP package during solder reflow, Microelectron. Reliab. 50 (7) (2010) 1014–1020.
[24] G. Hu, A.A.O. Tay, J. Luan, Y. Ma, Numerical and experimental study of interface delamination in flip chip BGA package, J. Electron. Packag. 132 (1) (2010), 011006.
[25] J. Galloway, B. Miles, Moisture absorption and desorption predictions for plastic ball grid array packages, IEEE Trans. Compon. Packag. Manuf. Technol. A 20 (3) (1997) 274–279.
[26] A.A.O. Tay, T.Y. Lin, Moisture diffusion and heat transfer in plastic IC packages, IEEE Trans. Compon. Packag. Manuf. Technol. A 19 (2) (1996) 186–193.
[27] E.H. Wong, Y.C. Teo, T.B. Lim, Moisture diffusion and vapor pressure modeling of IC packaging, 48th Elect. Compon. Technol. Conf 1998, pp. 1372–1378.
[28] S. Yoon, B. Han, Z. Wang, On moisture diffusion modeling using thermal-moisture analogy, J. Electron. Packag. 129 (4) (2007) 421–426.
[29] E.H. Wong, K.C. Chan, T.Y. Tee, R. Rajoo, Comprehensive treatment of moisture induced failure in IC packaging, Proc. 3rd Int. Electron. Manufact. Technol 1999, pp. 176–181.
[30] E.H. Wong, R. Rajoo, Moisture absorption and diffusion characterization of packaging materials—advanced treatment, Microelectron. Reliab. 43 (12) (2003) 2087–2096.
[31] C. Jang, B. Han, S. Yoon, Comprehensive moisture diffusion characteristics of epoxy molding compounds over solder reflow process temperature, IEEE Trans. Comp. Packag. Technol. 33 (4) (2010) 809–818.
[32] A. Mavinkurve, J.L.M.L. Martinez, M. van Soestbergen, J.J.M. Zaal, Moisture absorption by molding compounds under extreme conditions: impact on accelerated reliability tests, Microelectron. Reliab. 64 (2016) 254–258.
[33] D. Liu, S. Park, A note on the normalized approach to simulating moisture diffusion in a multimaterial system under transient thermal conditions using Ansys 14 and 14.5, J. Electron. Packag. 136 (3) (2014) 034501.
[34] J.N. Reddy, An Introduction to the Finite Element Method, third ed. McGraw-Hill, 2006.
[35] ANSYS, ANSYS Mechanical APDL Theory Reference, Release 15.0, Ansys, Inc., Canonsburg, PA, 2013.
[36] ANSYS, ANSYS Mechanical APDL Theory Reference, Release 17.0, Ansys, Inc., Canonsburg, PA, 2016.
[37] C. Jang, S. Park, B. Han, S. Yoon, Advanced thermal-moisture analogy scheme for anisothermal moisture diffusion problem, J. Electron. Packag. 130 (1) (2008), 011004.
[38] B. Xie, X. Fan, X. Shi, H. Ding, Direct concentration approach of moisture diffusion and whole-field vapor pressure modeling for reflow process — part I: theory and numerical implementation, J. Electron. Packag. 131 (3) (2009), 031010.
[39] B. Xie, X. Fan, X. Shi, H. Ding, Direct concentration approach of moisture diffusion and whole-field vapor pressure modeling for reflow process—part II: application to 3D ultrathin stacked-die chip scale packages, J. Electron. Packag. 131 (3) (2009), 031011.
[40] D. Liu, J. Wang, R. Liu, S. Park, An examination on the direct concentration approach to simulating moisture diffusion in a multi-material system, Microelectron. Reliab. 60 (2016) 109–115.
[41] S. Silling, Reformulation of elasticity theory for discontinuities and long-range forces, J. Mech. Phys. Solids 48 (2000) 175–209.
[42] B. Kilic, E. Madenci, Peridynamic theory for thermomechanical analysis, IEEE Trans. Adv. Packag. 33 (1) (2010) 97–105.
[43] S. Oterkus, E. Madenci, E. Oterkus, Y. Hwang, J. Bae, S. Han, Hygro-thermo-mechanical analysis and failure prediction in electronic packages by using peridynamics, 64th Elect. Compon. Technol. Conf 2014, pp. 973–982.
[44] S.W. Han, C. Diyaroglu, S. Oterkus, E. Madenci, E. Oterkus, Y. Hwang, H. Seol, Peridynamic direct concentration approach by using ANSYS, 66th Elect. Compon. Technol. Conf 2016, pp. 544–549.
[45] S. Oterkus, E. Madenci, A. Agwai, Peridynamic thermal diffusion, J. Comput. Phys. 265 (2014) 71–96.
[46] E.H. Wong, S.W. Koh, K.H. Lee, R. Rajoo, Advanced moisture diffusion modeling & characterisation for electronic packaging, 52nd Elect. Compon. Technol. Conf 2002, pp. 1297–1303.
[47] E.H. Wong, S.W. Koh, K.H. Lee, R. Rajoo, Comprehensive treatment of moisture induced failure – recent advances, IEEE Trans. Electron. Packag. Manuf. 25 (2002) 223–230.
[48] L. Zhu, D. Monthei, G. Lambird, W. Holgado, Moisture diffusion modeling and application in a 3D RF module subject to moisture absorption and desorption loads, 11th EuroSimE 2010, pp. 1–6.
[49] T. Ikeda, T. Mizutani, N. Miyazaki, Hygro-mechanical analysis of LCD panels, ASME Interpack 2009, p. 89267.
[50] E.H. Wong, The fundamentals of thermal-mass diffusion analogy, Microelectron. Reliab. 55 (3) (2015) 588–595.